ICES Journal of Marine Science, 62: 1636–1646 (2005)
doi:10.1016/j.icesjms.2005.06.008

An improved multiple-frequency method for measuring *in situ* target strengths

Stéphane G. Conti, David A. Demer, Michael A. Soule, and Jean H. E. Conti

Conti, S. G., Demer, D. A., Soule, M. A., and Conti, J. H. E. 2005. An improved multiple-frequency method for measuring *in situ* target strengths. – ICES Journal of Marine Science, 62: 1636–1646.

Refinements have been made to the multiple-frequency method for rejecting overlapping echoes when making target-strength measurements with split-beam echosounders described in Demer *et al*. (1999). The technique requires that echoes, simultaneously detected with two or more adjacent split-beam transducers of different frequencies, pass multiple-target rejection algorithms at each frequency, *and* characterize virtually identical three-dimensional target coordinates. To translate the coordinates into a common reference system for comparison, the previous method only considered relative transducer positions and assumed that the beam axes of the transducers were parallel. The method was improved by first, optimizing the accuracy and precision of the range and angular measurements of the individual frequency detections; and second, precisely determining acoustically the relative positions and angular orientations of the transducers, thus completely describing the reference-system transformation(s). Algorithms are presented for accurately and precisely estimating the transformation parameters, and efficiently rejecting multiple targets while retaining measurements of most single targets. These improvements are demonstrated through simulations, controlled test-tank experiments, and shipboard measurements using 38- and 120-kHz split-beam transducers. The results indicate that the improved multiple-frequency TS method can reject more than 97% of multiple targets, while allowing 99% of the resolvable single targets to be measured.

Keywords: split-beam, target strength, three-dimensional reference transformation.

Received 14 February 2005; accepted 1 June 2005.

S. G. Conti and D. A. Demer: Southwest Fisheries Science Center, 8604 La Jolla Shores Drive, La Jolla, CA 92037, USA. M. A. Soule: Fisheries Resource Surveys, PO Box 31306, Tokai 7966, Cape Town, South Africa. J. H. E. Conti: 69 Voie Antique, 69126, Brindas, France. Correspondence to S. G. Conti: tel: +1 858 534 7792; fax: +1 858 546 5652; e-mail: sconti@ucsd.edu.

Introduction

In acoustic surveys of aquatic organisms, a probability density function (pdf) of areal densities of scatterer type "x" ($P\{\rho_x\}$) can be estimated from the pdf of the integrated volume-backscattering coefficients ($P\{s_{A_x}\}$), or the total-backscattering, cross-sectional area per unit of sea surface area (m^2/km^2) from type-x animals, divided by the pdf of backscattering, cross-sectional areas from an individual type-x animal ($P\{\sigma_{bs_x}\}$):

$$P\{\rho_x\} = \frac{P\{s_{A_x}\}}{P\{\sigma_{bs_x}\}}. \quad (1)$$

The key to this measurement is the variable called "target strength" [$TS_x = 10 \log(\sigma_{bs_x})$]. TS_x is a non-linear function of the transmit frequencies, the distributions of animal sizes, shapes and orientations, and the acoustic properties of the animals relative to the surrounding medium. As these parameters may change in relation to survey locations and times, *in situ* measurements of TS_x may provide the best estimates of $P\{\sigma_{bs_x}\}$.

A multiple-frequency method has been developed that greatly enhances the accuracy and precision of *in situ* TS measurements using split-beam echosounders (Demer *et al*., 1999). The method improves the rejection of unresolvable and constructively interfering target multiples by combining the synchronized signals from two or more adjacent split-beam transducers of different frequencies which are not integer multiples of each other. The technique requires that simultaneously detected echoes

1054-3139/$30.00

pass multiple-target rejection algorithms at each frequency (based upon minimum echo amplitude, maximum off-axis detection angle, minimum and maximum echo duration and maximum sample-to-sample phase deviation; SIMRAD, 1996; Table 1), *and* characterize virtually identical three-dimensional (3-D) target coordinates. Thus, it is possible to make high-quality, multiple-frequency TS measurements concurrent with echo-integration surveys for the purposes of taxa identification and the estimation of animal abundance. This technique can also be used for other applications such as fish counting or target tracking.

Demer *et al.* (1999) showed that the primary limitations to the multiple-frequency TS method are errors in first, the 3-D target coordinates; and second, the 3-D target positional transformations between transducer reference systems. The errors in 3-D target coordinates are subject to the accuracy of the phase measurements, which are limited by the transducer characteristics (aperture, shading, and beam width), the phase-detection method, and the signal-to-noise ratio (SNR; primarily a function of the detection range, ambient noise, and receiver bandwidth). The uncertainty in translating 3-D target positions from one transducer reference system to another is limited by incomplete knowledge of the relative transducer-mounting geometries (Figure 1).

Uncertainty in 3-D target coordinates

The split-beam echosounder estimates the 3-D target position with estimates of range and two orthogonal off-axis angles. The measurement precision for radial range ($r = c/2SR$) is a function of the sampling rate of the echosounder (SR) and the sound speed (c). The accuracy of the radial-range measurement must be determined empirically as it depends upon estimates of sound speed and the two-way propagation delay ($t_{2\text{-way}}$), the latter being affected by the system-dependent echo-pulse rise time and delay in the receiving electronics (MacLennan, 1987).

In high signal-to-noise ratio (SNR) conditions, the precision of the off-axis angle measurements ($=\Delta\gamma_e/\Lambda$) is determined by the resolution of the detected electrical phase ($\Delta\gamma_e$), and the angle sensitivity (Λ) for converting electrical phase angles measured from the split-beam transducer halves (γ_e) to spatial angles between the beam axes and the target (α, alongship; and β, athwartship). For a fixed frequency (f) and TS, the SNR is primarily dependent upon range due to the associated attenuation from spreading and absorption. Thus, in field applications of the *in situ* TS measurement techniques, detection ranges should be limited to those with adequate SNR to allow maximal angular measurement precision (see Demer *et al.*, 1999).

Table 1. Multiple-target rejection criteria in the single-frequency, split-beam measurements. Unresolvable targets are filtered, to some extent, by imposing: (i) a minimum target strength; (ii) minimum and maximum duration of the echo envelope, normalized by the pulse length (τ); (iii) maximum one-way beam compensation; and (iv) a maximum sample-to-sample deviation of the phase measurements.

Minimum target strength (TS)	−90 dB
Minimum echo length	0.8τ (s)
Maximum echo length	1.5τ (s)
Maximum beam compensation [$\hat{B}(\alpha, \beta)$]	4 dB
Maximum phase deviation (P_{dev})	Four steps (1 step = 2.8125° elec.)

The accuracies of α and β measurements are primarily dependent upon the accuracies of the angle-sensitivity estimates [$\Lambda = (2\pi f/c)d_{eff}$], which are dependent upon f, c, and the effective distances between the transducer halves (d_{eff}). For symmetrical transducer halves with n elements each, d_{eff} can be estimated from the amplitude shading and spacing of the elements (Bodholt, 1991); notably, it is a non-linear function of c, α, and β. Constant Λ values (Table 2) only approximate the non-linear functions; their usage can cause inaccuracies in both phase-angle interpretation and the associated beam compensation.

The estimated off-axis angles (α and β) are used in conjunction with *a priori* knowledge of the transducer beam shape, beam width (γ), and beam-offsets or off-axis angular positions of the axis (α_o, β_o) to estimate the two-way compensation, $2B(\alpha, \alpha_o, \beta, \beta_o)$ (Bodholt and Solli, 1992), which is added to the beam-uncompensated measurements (TS_U):

$$TS = TS_U + 2B(\alpha, \alpha_o, \beta, \beta_o) \tag{2}$$

where

$$B(\alpha, \alpha_o, \beta, \beta_o) = -3\left[\left(\frac{\alpha-\alpha_o}{\gamma/2}\right)^2 + \left(\frac{\beta-\beta_o}{\gamma/2}\right)^2 - 0.18\left(\frac{\alpha-\alpha_o}{\gamma/2}\right)^2\left(\frac{\beta-\beta_o}{\gamma/2}\right)^2\right] \tag{3}$$

thus normalizing to the calibrated beam-axis. In the approximate beam shape described by Equation (3), the factor −0.18 mostly compensates TS for the differences between the actual non-linear Λ and the constant Λ typically used. However, the estimated 3-D positions retain some degree of error. Corresponding single-beam TS_U measurements can be compensated by evaluating Equation (3) with detection angles spatially transformed from concurrently detected, split-beam measurements (Demer *et al.*, 1999), where γ, α_o, and β_o are estimated for the single-beam transducer(s). For split- and single-beam transducers alike, small errors in the estimates of γ, α_o, and β_o can cause appreciable TS measurement uncertainty (Figure 2).

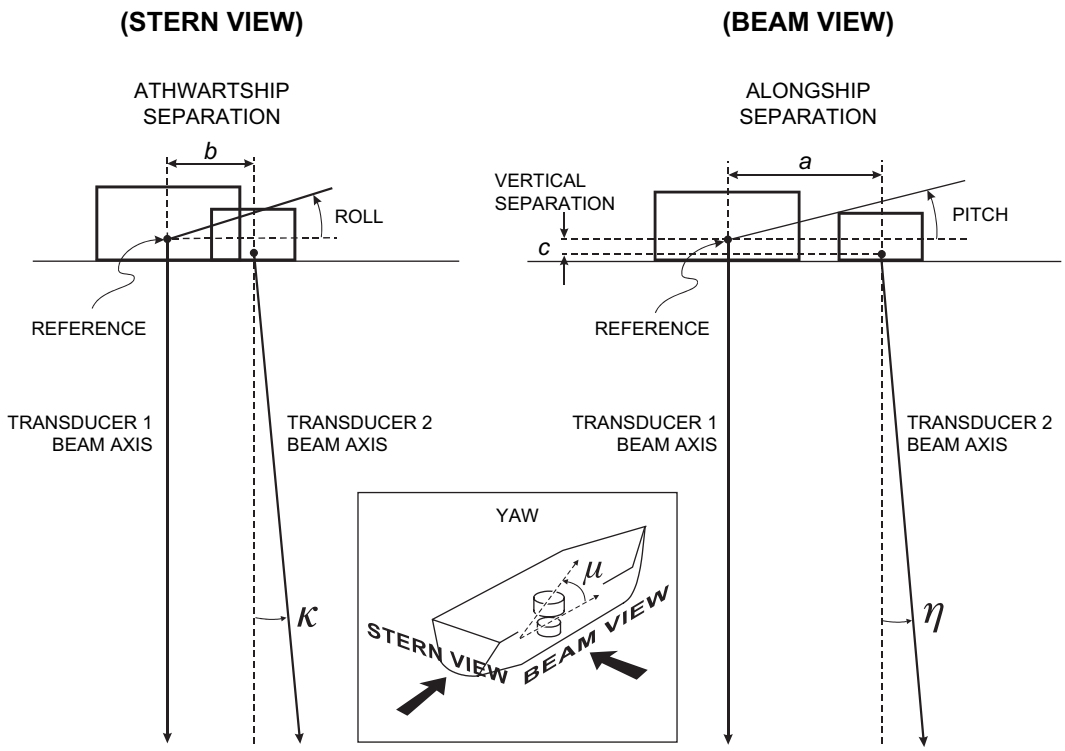

Figure 1. The 3-D target position detected with one frequency can be matched to the position detected by another frequency. The accuracy of the positioning is limited by the knowledge of the relative mounting geometries (a, b, and c transducer spacings, pitch and roll angles, and rotation of one transducer to another, yaw angle).

Uncertainty in transducer reference-system transformations

The multi-frequency method for single-target detection (multiple-target rejection) uses multiple transducers, typically juxtaposed rather than co-located. The transducer positions and beam axes define their own spatial reference systems that are translated in space and rotated relative to one another. To determine if targets perceived by two split-beam echosounders of differing frequencies corresponds to one target, or multiple unresolvable and interfering targets, the 3-D positions of the targets must be transformed into a common reference system for comparison. Demer *et al.*

Table 2. Nominal and calibrated (in parenthesis) echosounder and transducer specifications.

	Tank experiments		Ship experiments	
SIMRAD EK500	38 kHz	120 kHz	38 kHz	120 kHz
Actual frequency	37.878 kHz	119.047 kHz	37.878 kHz	119.047 kHz
Transducer model	ES38-7	ES120-7	ES38-12	ES120-7
TS gain (dB)	26.35	24.53	22.36	25.26
Beam width alongship (°)	6.8	7.4	12.0	7.3
Beam width athwartship (°)	6.8	7.5	12.0	7.2
Offset angle alongship (°)	0.0	−0.03	0.03	−0.01
Offset angle athwartship (°)	−0.1	−0.02	−0.1	0.04
Angle sensitivity (Λ)	22.1 (22.9)	21.5 (21.0)	12.5	21.0
Angular resolution (ζ; °)	0.13	0.13	0.23	0.13
Range resolution (m)	0.10	0.03	0.10	0.03
Pulse duration (τ; ms)	1.0	1.0	1.0	1.0
Receiver bandwidth (kHz)	3.8	12.0	3.8	12.0
Transmit power (kW)	2	1	1	1

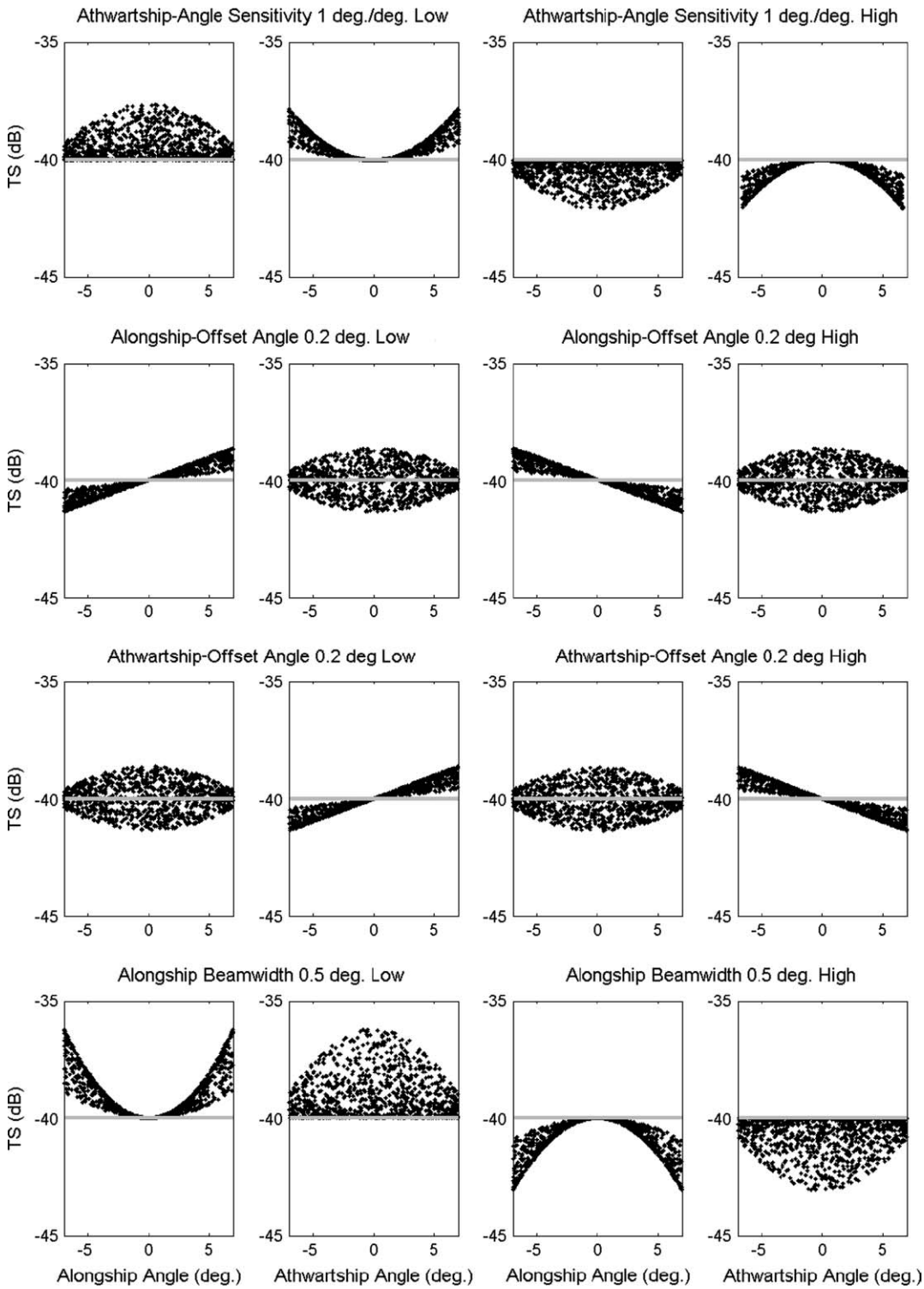

Figure 2. Simulation of a −40 dB target randomly positioned 1000 times in the beam and compensated using Equation (3). Perfect compensation would result in constant target-strength values vs. off-axis angles. Variations in TS indicate that minor errors in the transducer-angle sensitivity, the beam-offset angles, and the beam width parameters (i.e. settings too high or low relative optimal) can cause relatively major biases and imprecision in the resulting TS measurements. Errors in angle sensitivity and beam width parameters are indistinguishable from this analysis.

(1999) took account of reference-system translations, and acknowledged the potential importance of angular transformations, but for simplicity assumed that the beams were parallel (i.e. did not account for reference-system rotations). To more accurately transform the reference systems, estimates are needed for six geometrical parameters (translations a, b, and c, and rotations η, κ, and μ; Figure 1). This paper presents an algorithm for accurately, precisely, and simultaneously estimating all of these parameters from measurements with a standard target. The resulting improved performance of the multiple-frequency method for multiple-target rejection is then demonstrated empirically under both laboratory and field conditions. Throughout this study, a system SIMRAD ES38-12 or ES38-7, and ES120-7 transducers were used in the tank experiments and in the field, as well as in Demer *et al.* (1999). Therefore, this system was chosen as a benchmark to evaluate the technique presented here, and to compare it with the results obtained by Demer *et al.* (1999). It has to be noted that this technique can be applied to any echosounder providing simultaneous measurements for all the transducers.

Methods

Coordinate-system transformations

Consider two transducers T_1 and T_2, having reference systems R_1 $(\vec{X}_1, \vec{Y}_1, \vec{Z}_1)$and R_2 $(\vec{X}_2, \vec{Y}_2, \vec{Z}_2)$, respectively. Choosing R_1 to be the common reference, a transformation from R_2 to R_1 is required. The origins O_2 of R_2 and O_1 of R_1 are separated by a, b, and c along the axes X_1, Y_1, and Z_1, respectively (Figure 1). The axes of R_2 are rotated relative to those of R_1 as described using the Euler angles ϕ, θ, and ψ (Peres, 1962; Figure 3a). The Cartesian coordinates of the R_2 axes in R_1 are:

$$\vec{X}_2 = \begin{bmatrix} \cos\phi\cos\psi - \sin\phi\cos\psi\cos\theta \\ -\sin\phi\cos\psi - \cos\phi\sin\psi\cos\theta \\ \sin\psi\sin\theta \end{bmatrix}_{R_1}$$

$$\vec{Y}_2 = \begin{bmatrix} \cos\phi\sin\psi + \sin\phi\cos\psi\cos\theta \\ -\sin\phi\sin\psi + \cos\phi\cos\psi\cos\theta \\ -\cos\psi\sin\theta \end{bmatrix}_{R_1}$$

$$\vec{Z}_2 = \begin{bmatrix} \sin\phi\sin\theta \\ \cos\phi\sin\theta \\ \cos\theta \end{bmatrix}_{R_1} \quad (4)$$

The target M is measured by T_1 in R_1, and T_2 in R_2. The Cartesian coordinates of the measured positions M_1 in R_1, and M_2 in R_2 are:

$$\vec{M}_1 = \begin{bmatrix} x_1 \\ y_1 \\ z_1 \end{bmatrix}_{R_1} = \frac{r_1}{\sqrt{1 - \sin^2\alpha_1 \sin^2\beta_1}} \begin{bmatrix} \sin\alpha_1\cos\beta_1 \\ \cos\alpha_1\sin\beta_1 \\ \cos\alpha_1\cos\beta_1 \end{bmatrix}_{R_1} \quad (5)$$

$$\vec{M}_2 = \begin{bmatrix} x_2 \\ y_2 \\ z_2 \end{bmatrix}_{R_2} = \frac{r_2}{\sqrt{1 - \sin^2\alpha_2 \sin^2\beta_2}} \begin{bmatrix} \sin\alpha_2\cos\beta_2 \\ \cos\alpha_2\sin\beta_2 \\ \cos\alpha_2\cos\beta_2 \end{bmatrix}_{R_2} \quad (6)$$

where (r_1, α_1, β_1) and (r_2, α_2, β_2) describe the position of M (range, alongship angle, athwartship angle) as measured by the echosounders T_1 and T_2 in R_1 and R_2, respectively (Figure 3b).

The transformation H to obtain the Cartesian coordinates of the point $\vec{M}_1(x_1, y_1, z_1)_{R_1}$ in R_1 from the coordinates of $\vec{M}_2(x_2, y_2, z_2)_{R_2}$ in R_2 is:

$$\vec{M}_1 = H(\vec{M}_2) = \vec{T} + R \cdot \vec{M}_2 \quad (7)$$

$$\vec{T} = \vec{O}_2 = \begin{bmatrix} a \\ b \\ c \end{bmatrix}_{R_1} \quad (8)$$

$$R = \begin{bmatrix} \vec{X}_2\cdot\vec{X}_1 & \vec{Y}_2\cdot\vec{X}_1 & \vec{Z}_2\cdot\vec{X}_1 \\ \vec{X}_2\cdot\vec{Y}_1 & \vec{Y}_2\cdot\vec{Y}_1 & \vec{Z}_2\cdot\vec{Y}_1 \\ \vec{X}_2\cdot\vec{Z}_1 & \vec{Y}_2\cdot\vec{Z}_1 & \vec{Z}_2\cdot\vec{Z}_1 \end{bmatrix} \quad (9)$$

where $\vec{T}$ is the translation of O_2 to O_1, and R is the rotation matrix of R_2 to R_1. The pitch (η), roll (κ), and yaw (μ) angles between T_1 and T_2 (Figure 3c) are:

$$\eta = \cos^{-1}(\vec{X}_1 \cdot \vec{X}_2) \quad (10)$$

$$\kappa = \cos^{-1}(\vec{Y}_1 \cdot \vec{Y}_2) \quad (11)$$

$$\mu = \cos^{-1}(\vec{Z}_1 \cdot \vec{Z}_2). \quad (12)$$

The diagonal elements of R depend only on these three angles:

$$R = \begin{bmatrix} \cos\eta & \cdot & \cdot \\ \cdot & \cos\kappa & \cdot \\ \cdot & \cdot & \cos\mu \end{bmatrix}. \quad (13)$$

Thus, if the Euler angles ϕ, θ, and ψ, and translations a, b, and c between R_1 and R_2 are known, then H can be determined analytically. Usually, however, the relative positions of the transducers and the relative orientations of their beam axes are not known. Therefore, the parameters of H can be estimated using an ensemble of N positions i of a single target measured simultaneously by the two transducers T_1 and T_2 with overlapping beam patterns (i.e. r_{1i}, α_{1i}, β_{1i}, r_{2i}, α_{2i}, and β_{2i}), and a non-linear optimization scheme. The N sets of positions for M_2 (r_{2i}, α_{2i}, β_{2i}) are transformed to R_1 using Equation (7), a non-linear, least-squares, optimization algorithm (*lsqnonlin*; The Mathworks, Optimization Toolbox v2.1.1, 2002), and

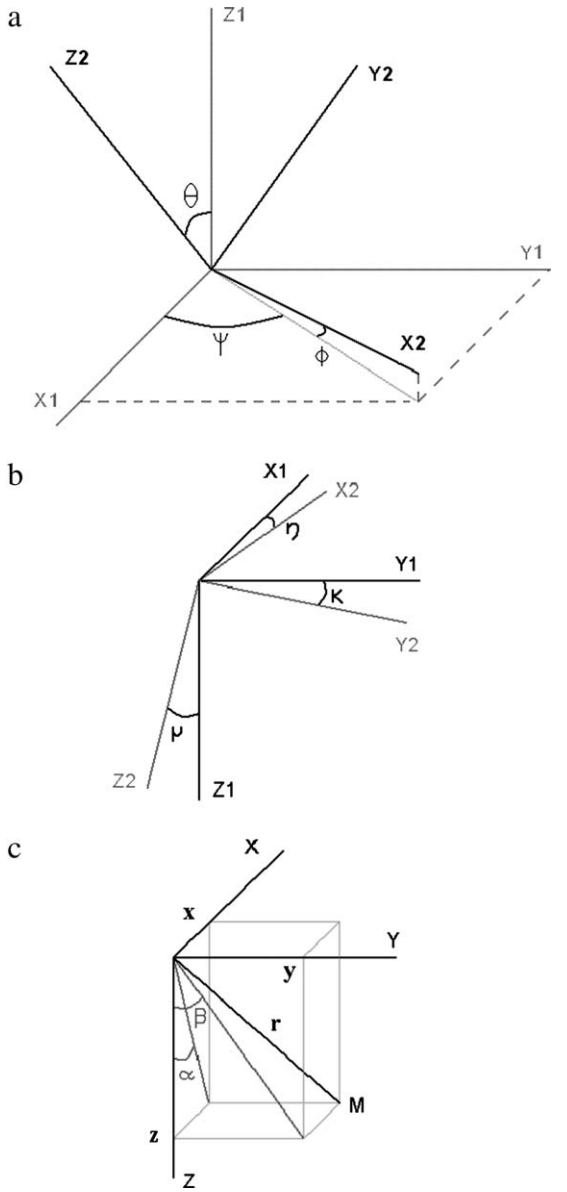

Figure 3. Definition of the Euler angles ϕ, θ, and ψ between R_1 and R_2 for the transformation from R_2 to R_1 (a); definition of the pitch angle η, roll angle κ, and yaw angle μ between the axes $(\vec{X}_1, \vec{Y}_1, \vec{Z}_1)$ and $(\vec{X}_2, \vec{Y}_2, \vec{Z}_2)$ of R_1 and R_2, respectively (b); and definition of the coordinates of the target $\vec{M}(x, y, z)$ in a 3-D coordinate system $(\vec{X}, \vec{Y}, \vec{Z})$, with the measurements from an echosounder r, α, and β(c).

a set of initial parameters. The resulting sets of positions (r'_{2i}, α'_{2i}, and β'_{2i}) are then compared with the temporally matching M_1 positions (r_{1i}, α_{1i}, and β_{1i}).

For a low number of target positions ($N < 3$), the system is underdetermined (each position provides three equations, one for each axis, for six unknowns). In this case, *lsqnonlin* employs a medium-scale algorithm based on the Levenberg–Marquardt method with line search (Levenberg, 1944; Marquardt, 1963; Moré, 1977). The line-search algorithm is a mixed quadratic and cubic polynomial interpolation and extrapolation algorithm. When $N \geq 3$, the system is completely determined and *lsqnonlin* uses a large-scale version of the algorithm (Coleman and Li, 1994, 1996). In this case, each iteration involves the approximate solution of a large linear system using the method of preconditioned conjugate gradients. The criteria for this optimization algorithm must be of the form $f(x) = f_1(x)^2 + f_2(x)^2 + \ldots + f_I(x)^2$, with I Equations. Here, the minimization considers the criteria C of the N distances between M_{1i} in R_1 and M_{2i} in R_1 along all three axes:

$$C(a,b,c,\phi,\theta,\psi) = \sum_{i=1}^{N} \left\| \begin{bmatrix} x_{1i} \\ y_{1i} \\ z_{1i} \end{bmatrix}_{R_1} - \vec{T} - R \begin{bmatrix} x_{2i} \\ y_{2i} \\ z_{2i} \end{bmatrix}_{R_2} \right\|_2^2 \tag{14}$$

where $\| \|_2$ designates the l_2-norm of the vector ($\|[x, y, z]\|_2 = \sqrt{x^2 + y^2 + z^2}$). The number of equations of the system defined by C is 3N.

The determination of geometrical parameters is repeated K times for K ensembles of N positions of the target. The parameters are determined by the average of the K realizations. If more than two transducers are employed, the parameter estimations are performed pairwise.

Multiple-target rejection

To reject measurements of multiple targets falsely identified as individual targets by one or more echosounders, the multiple-frequency method requires that the estimated 3-D positions of the detected targets occupy virtually the same space. To facilitate this requirement, the position of each target detected by T_2 is transformed into the T_1 reference using the geometrical parameters determined with a single target as discussed above. The root-mean-square differences of the range r, the alongship angle α, and athwartship angle β (δr, $\delta\alpha$, and $\delta\beta$, respectively), are then compared with arbitrary threshold values. If one of the three root-mean-square differences is greater than the corresponding threshold value, the detected target is rejected. Rectangular-box rejection criteria were used, similar to the one in Demer *et al.* (1999), in order to compare the results from the two techniques. The threshold values are chosen according to desired acceptance and rejection percentages (goal: >95% acceptance of single targets and >95% rejection of multiple targets). Different rejection criteria could be proposed, such as elliptical criteria, and may best suit the problem.

Simulations

A simulation was performed to test the effectiveness of estimating the geometrical parameters between two transducers. Realistic values were selected for a, b, c, ϕ, θ, and ψ (0.4 m, 0.1 m, 0.1 m, $-2°$, $3°$, and $-4°$, respectively), and a matrix R was calculated using Equations (4) and (9). This matrix was inverted to obtain the transformation from R_1 to R_2. An ensemble of N positions $\vec{M}_1$ ($\vec{M}_{1i}$, with i ranging from 1 to N) were randomly generated from a uniform distributions of r_{1i}, α_{1i}, and β_{1i}, confined to the overlapping portions of $12°$ and $7°$ beam widths (simulating the SIMRAD ES38-12 and ES120-7 transducers) for three different cases of target positions. To simulate $\vec{M}_{2i}$, the $\vec{M}_{1i}$ were transformed to R_2 by:

$$\vec{M}_{2i} = R^{-1} \cdot (\vec{M}_{1i} - \vec{T}), \quad (15)$$

and converted to r_{2i}, α_{2i}, and β_{2i}.

To account for the precision of the range and angle measurements at various signal-to-noise ratios, random noise was added independently to $\vec{M}_{1i}$ and $\vec{M}_{2i}$. The magnitude of the noise corresponded to the signal-to-noise ratio as defined in Demer *et al.* (1999, Table 3). The parameters were estimated either for signal-to-noise ratios ranging from 18 to 32 dB, and the corresponding precision of the alongship and athwartship angles from Table 3, or for a signal-to-noise ratio of 32 dB corresponding to the maximum measurement precision. Since the measurement precision in range does not change significantly with decreasing signal-to-noise ratios, the same value was used for signal-to-noise ratios between 18 and 32 dB.

Thus, sets of simulated data were generated, corresponding to three different cases:

Case 1: the target positions were confined between 5 and 10 m and 20−50 m, without noise and for signal-to-noise ratios ranging from 18 to 32 dB;

Case 2: the target positions were confined to a constant range at either 5 or 20 m, without noise and a signal-to-noise ratio of 32 dB; and

Case 3: the target position is confined to constant angles of $\alpha_1 = 2°$ and $\beta_1 = 2°$, while the range was varied between 5 and 10 m or between 20 and 50 m, without noise and for a signal-to-noise ratio of 32 dB.

In all three cases, 1000 random-target positions were simulated and the parameters a, b, c, ϕ, θ, and ψ were estimated with N varying between 1 and 200, for K = 100. Using all 1000 positions, the root-mean-square difference between M_{2i} and M_{1i} in R_1 provided estimates for δr, $\delta\alpha$, and $\delta\beta$, which were compared with the measurement precision of the echosounder.

Table 3. Signal-to-noise ratios and corresponding measurement precision of target range and off-axis angles for a SIMRAD EK500 configured with SIMRAD ES38-12 and ES120-7 transducers (Demer *et al.*, 1999).

Transducer SNR (dB)	ES38-12		ES120-7	
	Range (m)	Angle (°)	Range (m)	Angle (°)
32	0.1	0.23	0.03	0.13
26	0.1	0.45	0.03	0.27
23	0.1	0.68	0.03	0.4
20	0.1	0.9	0.03	0.54
18	0.1	1.13	0.03	0.67

Experiments

Next, actual geometrical parameters (a, b, c, ϕ, θ, and ψ) were estimated using 3-D positional measurements of a single 38.1-mm diameter, tungsten-carbide sphere (WC, with 6% cobalt binder) that was randomly moved around overlapping transducer beams. In addition, as a test of the multi-frequency, multiple-target rejection algorithm, two 38.1-mm diameter WC spheres were independently moved within the same overlapping beams but confined to the resolution volume of the echosounder. The parameter estimation experiments were conducted first in a large test tank at the Institute of Maritime Technology (IMT) in Simonstown, South Africa, from 13 November to 4 December 1998; and second, aboard RV "Yuzhmorgeologiya" anchored in Martel Inlet, King George Island, Antarctica, 1 March 2001. Tests of the multiple-frequency, multiple-target rejection algorithm were conducted only at IMT, because such controlled tests with multiple targets could not be realized *in situ*. The echosounder used in all of these experiments was the SIMRAD EK500 (Bodholt *et al.*, 1989; firmware version 5.3), synchronously transmitting 1-ms pulses from 38- and 120-kHz split-beam transducers.

Parameter estimations in a tank

The IMT tank (approximately 20 m long by 10 m wide by 10 m deep), contained freshwater at a temperature of 19.9 °C ($c \cong 1492\ ms^{-1}$; absorption coefficients = 1.05, and 5 $dBkm^{-1}$, respectively). The transducers (SIMRAD ES38-7 and ES120-7) were mounted next to each other, 4 m deep and 6 m from one end of the tank, projecting horizontally down the length of the tank, with beam axes focused at a range of 4.76 m.

First, the performance of the split-beam system for measuring 3-D target positions and TS was characterized and optimized. The radial range from the face of each transducer to a 38.1-mm WC sphere was measured with a tape to be 4.76 $\pm$ 0.01 m. The mean radial ranges were then measured using each echosounder frequency. Then,

the angle sensitivities and the beam angles were measured. For both the ES38-B and ES120-7 transducers, the WC sphere was moved to off-axis distances of 0 m (0.0°), 0.232 m (2.8°), and 0.325 m (3.9°) while maintaining the range at 4.76 ± 0.01 m. The system's Λ settings were then adjusted until the measurements of α and β were correct.

Using these revised values for the Λ settings, both the 38- and the 120-kHz systems were calibrated using the standard-sphere method (Foote, 1990) for determining on-axis system gain and a 3-D, curve-fitting programme (Lobe.exe, Simrad, 1996) that employs Equation (3) for determining beam-directionality parameters (see Table 2). Ultimately, the sphere TS measurements should be independent of detection angle. Therefore, the values for Λ, γ_o, β_o, and ϕ were further refined by minimizing the first two coefficients of second-order polynomial fits to TS(α) and TS(β):

$$TS = A_1\alpha^2 + A_2\alpha + A_3 \text{ and } TS = B_1\beta^2 + B_2\beta + B_3, \qquad (16)$$

where TS is the beam-compensated measurement made along the alongship and athwartship axes, respectively. Consistent with the analysis shown in Figure 2, the associated transducer-beam angles were adjusted if coefficients A_1 or B_1 were appreciably non-zero; and the associated off-axis angles were adjusted if coefficients A_2 or B_2 were appreciably non-zero.

Then, 3-D target positions were simultaneously measured by moving a single 38.1-mm WC sphere within the overlapping beams. The relative transducer-mounting geometries were characterized as described earlier using N from 1 to 700, for K = 100, see the section "Multiple-target rejection in a tank".

Using the echosounder configuration described in the previous experiment, and the transformation parameters determined with N = 500 and K = 100, the effectiveness of the EK500 and multiple-frequency algorithms for rejecting multiple targets were evaluated by moving two WC spheres randomly within the same resolution volume. To determine the optimal performance of the multiple-frequency algorithm, the δr, δα, and δβ were thresholded with a variety of values.

Parameter estimations at sea

The echosounder transducers (SIMRAD ES38-12 and ES120-7) were mounted next to each other in a steel blister on the hull of RV "Yuzhmorgeologiya". The transducer faces were positioned down-looking at a nominal depth of 5 m. A single 38.1-mm WC sphere was suspended beneath the ship by three monofilament lines, and moved extensively within the overlapping main-lobes of the 38 and 120 kHz transducers. Repeating this at target ranges of 20, 30, 40, and 50 m yielded 14 293 pairs of 3-D target positions.

The next step was optimizing the accuracy and precision of the range and angular measurements of the individual frequency detections. The range error is minimized intrinsically via the transducer-coordinate transformation. To optimize the angular measurements, recall that Λ is dependent on the transducer-element weighting and spacing, and the acoustic wavelength. Because the wavelength changes as a function of sound speed, which changes as a function of water temperature, salinity, and pressure, both the Λ and γ can change between operating environments. Therefore, unless the exact position of the standard sphere is known from an independent measure, the measurements made during a standard-sphere calibration, even at different depths, cannot be used to simultaneously characterize these two parameters (i.e. the solution is underdetermined). Therefore, an optimization algorithm was used (see the section Parameter estimations in a tank, Equation (16), and Figure 2). The geometrical parameters were then determined using N from 1 to 1000, and for K = 100 ensembles of N positions.

Results

Simulation

For case 1, where the target positions were confined between 5 and 10 m or 20−50 m, the errors in parameter estimates without noise were practically zero for N > 3. With noise (SNR = 32 dB), the range error (δr) and the angle errors (δα, and δβ) converged with increasing N to 0.042 m, 0.1°, and 0.1°, respectively, for a 32 dB signal-to-noise ratio. The minimum errors with noise were obtained for N > ∼100, irrespective of the target range.

In case 1, the parameters between the transducers could be estimated precisely by using a sufficient number of target positions N until steady values were reached for signal-to-noise ratio ranging from 18 to 32 dB. For the same range of signal-to-noise ratio, the positional errors correspond to the precision of the measurements (Figure 4). The results shown in Figure 4 were obtained with N = 1000, allowing a good precision of the geometrical parameters for all signal-to-noise ratio values investigated.

For case 2, where the target positions were confined to a constant range at either 5 or 20 m; all three errors decreased vs. increasing N. Without noise, the errors were virtually 0 for N > 3. With noise (SNR = 32 dB), minimum errors were obtained for N > ∼100, more than in case 1. Again, the errors were 0.042 m, 0.1°, and 0.1° for δr, δα, and δβ, respectively, irrespective of the target range.

For case 3 where the target position was confined to constant angles of $\alpha_1 = 2°$ and $\beta_1 = 2°$, while the range was varied between 5 and 10 m or between 20 and 50 m, the results equalled those for case 2. Minimum errors were achieved for N > ∼100, irrespective of the target range.

In all three cases, the errors and the standard deviations of the errors reached steady minimum values in unison. In

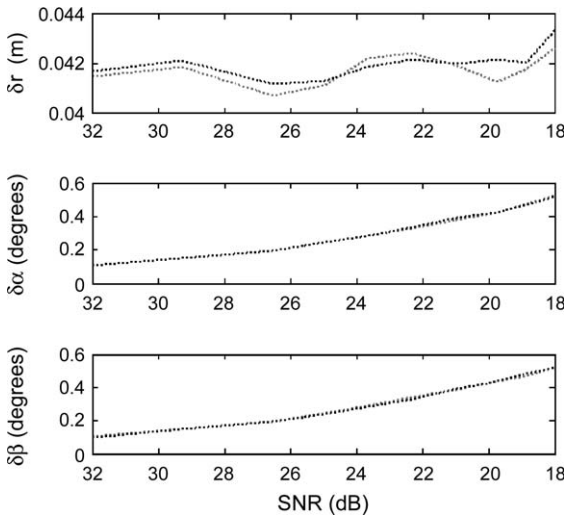

Figure 4. Positional errors vs. signal-to-noise ratio (SNR) for the case 1 of the simulation: the target positions were confined between 5 and 10 m (grey) and 20−50 m (black). For both ranges, K = 100 and N = 1000.

general, the estimated parameters stabilized to within 10% of their true values for N > 500, and K = 100. Larger N marginally increased the precision of the estimates of the geometrical parameters.

Parameter estimations in a tank

The mean radial ranges between the transducers and the sphere were measured using both echosounder frequencies ($\bar{r}$ = 5.0014 m at 38 kHz; and $\bar{r}$ = 4.9526 m at 120 kHz). Comparing this with the actual range of 4.76 ± 0.01 m, the mean-range biases were 0.24 m (2.44 samples), and 0.19 m (6.51 samples) at 38 and 120 kHz, respectively. Note, the EK500 firmware V5.2 and V5.3 uniformly subtracts three range samples and interpolates between range cells at all frequencies. This is done for the purpose of internal transmission-loss compensation only and is not reflected in the target-range data output by the echosounder. The nominal angle sensitivities for these transducers were measured to be $\Lambda_{38\ \mathrm{kHz}} = 22.1$ and $\Lambda_{120\ \mathrm{kHz}} = 21.5$ (differing 1−2.4% from the manufacturer's nominal values of 21.9 and 21.0, respectively).

Single-target detections with the EK500 single-frequency algorithm totalled 1820 and 828 out of 2000 pings, or 91% and 41.1% at 38 and 120 kHz, respectively, with reverberation in the tank causing a reduction in detection efficiency at 120 kHz. A total of 750 detection pairs was recorded simultaneously by both echosounders (90.6% of the 120 kHz detections). For N > ~100, δr, δα, and δβ reached steady-state minimums of ~0.01 m, 0.23° and 0.25°, respectively (Figure 5). Consistent with the simulation experiments, the parameters converged for N > ~500. Also, the estimated transformation parameters were very close to the values measured *a priori* from the geometry of the transducer-mounting apparatus (Table 4); slight discrepancies occurred mainly in the angular-transformation parameters.

Multiple-target rejection in a tank

The EK500, target, detection algorithm falsely misinterpreted two acoustically unresolvable 38.1-mm WC spheres as individuals in 316 and 242 of the 1000 pings (31.6% and 24.2%), at 38 and 120 kHz, respectively. Erroneous single-target detections were made simultaneously at both frequencies in 117 of the 1000 pings (11.7%).

Applying the new multiple-frequency method with different spatial-matching thresholds (δr, δα, and δβ), various combinations of rejection and acceptance levels were achieved (Table 5). For example, with δr = 0.027 m, and δα = δβ = 0.13°, the false-target rejection and acceptance rates were 97.2% and 99.0%, respectively.

For comparison with the original technique (Demer *et al.*, 1999), the same set of multiple-target data was tested without estimation of the rotational parameters (i.e. optimal account was taken only for reference-system translations). The rotation parameters φ, θ, and ψ were the nominal

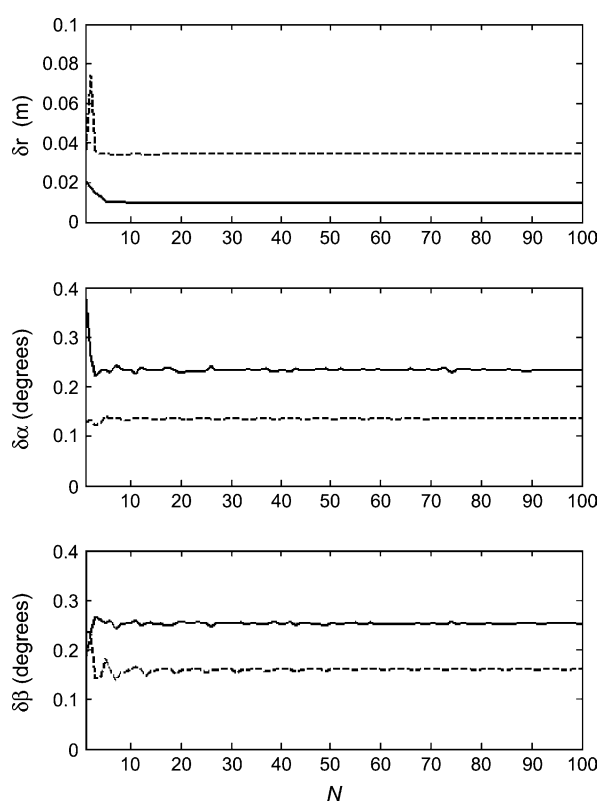

Figure 5. Positional errors vs. N for the transformations of the tank- and shipboard-target detections. To estimate the transformation parameters, the target was moved in the tank at a constant range of 5 m (solid), and beneath the ship at ranges varying from 20 to 40 m (dashed). For both experiments, K = 100.

Table 4. Known or nominal, and estimated transformation parameters for the simulation, tank, and ship experiments. For the simulations experiments with and without noise, the parameters were estimated with N = 1000. For the tank and shipboard experiments, the parameters were estimated with N = 700 and N = 1000, respectively. In all cases, K = 100.

Geometrical parameters		a (m)	b (m)	c (m)	ψ (°)	ϕ (°)	θ (°)
Simulation							
True parameters		0.40	0.10	0.10	3.00	−4.00	−2.00
Estimated parameters							
Case 1 without noise	Range 5−10 m	0.40	0.10	0.10	3.00	−4.00	−2.00
	Range 20−50 m	0.40	0.10	0.10	3.00	−4.00	−2.00
With noise	Range 5−10 m	0.40	0.10	0.08	2.99	−3.98	−2.02
	Range 20−50 m	0.38	0.10	0.08	3.01	−3.99	−2.01
Estimated parameters							
Case 2 without noise	Range 5 m	0.40	0.10	0.10	3.00	−4.00	−1.98
	Range 10 m	0.40	0.10	0.10	3.00	−4.00	−1.99
With noise	Range 5 m	0.40	0.11	0.09	3.30	−4.32	−2.20
	Range 10 m	0.39	0.08	0.08	3.03	−3.95	−1.98
Estimated parameters							
Case 3 without noise	Range 5−10 m	0.40	0.10	0.10	2.92	−3.79	−1.99
	Range 20−50 m	0.40	0.10	0.10	2.97	−3.93	−2.00
With noise	Range 5−10 m	0.40	0.11	0.08	2.97	−4.99	−2.06
	Range 20−50 m	0.40	0.11	0.09	2.70	−4.51	−2.06
Test tank							
Nominal parameters		0.00	−0.44	0.00	0.00	0.00	5.29
Estimated parameters		−0.05	−0.47	0.07	−1.31	1.71	5.09
Ship							
Nominal parameters		0.44	0.00	0.00	0.00	0.00	0.00
Estimated parameters		0.45	0.08	0.04	0.20	−2.57	0.42

parameters of the transducer mounting (Table 4). The translational parameters a, b, and c were estimated with N = 500 and K = 100. With these parameters and best-possible threshold values of $\delta r = 0.05$ m, and $\delta\alpha = \delta\beta = 0.8°$, the false-target rejection and acceptance rates were 94.6% and 99.0%, respectively. Therefore, adding the angular information between the transducers improved the false-target rejection and acceptance rates, compared with Demer *et al.* (1999).

Table 5. Various thresholds on range and angle errors, and their corresponding rates of single-target acceptance and multiple-target rejection. The acceptance rates were estimated for the 700 single-target detections recorded simultaneously at 38 and 120 kHz. The rejection rates were estimated for the 117 multiple-target detections recorded simultaneously at both frequencies over 1000 pings. Acceptance and rejection rates from Demer *et al.* (1999). The original method inherently accepts and rejects as many individual scatterers as the multiple-frequency methods, but is much worse at rejecting false targets (Demer *et al.*, 1999).

Range threshold (m)	Angular threshold (°)	Acceptance (%)	Rejection (%)
0.027	0.74	99.0	97.2
0.023	0.74	94.7	97.8
0.027	0.66	96.7	97.4
0.023	0.66	92.5	98.0
0.034	0.76	100.0	96.4
0.010	0.24	35.0	100.0
Demer *et al.* (1999)		99	94.6

Threshold values will be different depending on the SNR. For a given system of echosounders, SNR is modulated primarily by the target range and TS, and the ambient noise. The values given here are of interest in that they allow the new technique to be compared with the original, and for an evaluation to be made of the improvements it provides.

Parameter estimations at sea

For $N > \sim 100$, δr, $\delta\alpha$, and $\delta\beta$ reached steady-state minimums of 0.03 m, 0.13°, and 0.16°, respectively (Figure 5). These $\delta\alpha$ and $\delta\beta$ were higher than those from the test-tank experiments, despite a worse angular resolution for the shipboard 38-kHz transducer (0.23°) compared with the tank 38-kHz transducer (0.13°; see Table 2). Although the shipboard data were acquired for various and larger target ranges, which intuitively should improve estimation of the transformation parameters, the simulation experiments did not predict such improvements. Rather, the $\delta\alpha$ and $\delta\beta$ were smaller for the shipboard experiments

possibly because there was less reverberation noise compared with the test tank.

The estimated parameters were compared with the nominal values obtained from the drawing of the ship's transducer mounting (Table 4). Again, parameters estimated with $N > \sim 500$ are quite close to the nominal values though slight discrepancies occurred mainly in the angular-transformation parameters.

Conclusion

The multiple-frequency method improves the rejection of unresolvable and constructively interfering target multiples. The method has been improved by first, optimizing the accuracy and precision of the range and angular measurements of the individual frequency detections; and second, more precisely determining the relative three-dimensional 3-D locations and angular orientations of the transducers and thus the positional transformation. A new algorithm has been developed for accurately and precisely estimating these transformation parameters.

Without noise, three simulations employing the algorithm showed that the geometrical parameters between the transducers could be estimated almost perfectly. Also, the target positions measured by one transducer in one reference system could be transformed into the reference system of another transducer and identically match its corresponding target positions. With noise, the geometrical transformation parameters were still determined accurately enough to transform the target positions between reference systems to within the precision of the range and angular measurement of the echosounders at a specified signal-to-noise ratio. The accuracy of the parameter estimation increased with the number of target positions. As the signal-to-noise ratio decreases, the number of target positions required must be increased. Also, the parameter estimation was most efficient if the target positions included a variety of ranges and off-axis angles. The tank and shipboard experimental data showed the same general results.

Comparing the single-target experiment with the multiple-target experiment, δr was greater for false targets than single targets, while $\delta\alpha$ and $\delta\beta$ were similar for both. Thus, the range threshold was more powerful for rejecting multiple targets than the angular threshold. Applying thresholds of ± 0.027 m in radial range and $\pm 0.13°$ in off-axis angles, it was shown that $>99\%$ of resolvable single targets were accepted, while $>97\%$ of multiple targets were rejected.

Acknowledgements

This research was supported by the US Antarctic Marine Living Resources Program (AMLR), and the Sea Fisheries Research Institute, Cape Town, South Africa. Special thanks go to Manuel Barange and Merrick Whittle for graciously accommodating the test-tank experiments; and to Mark Prowse and Jennifer Emery for assisting with the shipboard experiments.

References

Bodholt, H. 1991. Split-beam transducer for target-strength measurement. Scandinavian Cooperation Meeting in Acoustics XIII. Ed. by H. Hobæk, Department of Physics. Science Technical Report, 227 (University of Bergen, Norway), p. 73.

Bodholt, H., Nes, H., and Solli, H. 1989. A new echosounder system. Proceedings of the Institute of Acoustics, 11(3): 123–130.

Bodholt, H., and Solli, H. 1992. Application of the split-beam technique for *in-situ*, target-strength measurements. *In* World Fisheries Congress, Athens. 21 pp.

Coleman, T. F., and Li, Y. 1994. On the convergence of reflective Newton methods for large-scale, nonlinear minimization subject to bounds. Mathematical Programming, 67-2: 189–224.

Coleman, T. F., and Li, Y. 1996. An interior, trust-region approach for nonlinear minimization subject to bounds. SIAM Journal on Optimization, 6: 418–445.

Demer, D. A., Soule, M. A., and Hewitt, R. P. 1999. A multiple-frequency method for potentially improving the accuracy and precision of *in situ* target-strength measurements. Journal of the Acoustical Society of America, 105(4): 2359–2376.

Foote, K. G. 1990. Spheres for calibrating an eleven-frequency, acoustic-measurement system. ICES Journal of Marine Science, 46: 284–286.

Levenberg, K. 1944. A method for the solution of certain problems in least-squares. Quarterly of Applied Mathematics, 2: 164–168.

MacLennan, D. N. 1987. Time-varied-gain functions for pulsed sonars. Journal of Sound and Vibration, 110: 511–522.

Marquardt, D. 1963. An algorithm for least-square-estimation of nonlinear parameters. SIAM Journal of Applied Mathematics, 11: 431–441.

Moré, J. J. 1977. The Levenberg–Marquardt algorithm: implementation and theory. *In* Numerical Analysis. Lecture Notes in Mathematics, vol. 630, pp. 105–116. Ed. by G. A. Watson. Springer, New York.

Peres, J. 1962. Mécanique Générale, 2nd edn. pp. 50–52. Ed. by Masson, Paris.

SIMRAD. 1996. Simrad EK500 Scientific Echosounder Instruction Manual. Simrad Subsea A/S, Horten, Norway.